Journal of Power Sources 218 (2012) 237–243

Contents lists available at SciVerse ScienceDirect

Journal of Power Sources

journal homepage: www.elsevier.com/locate/jpowsour

The influence of incorporating MgO into Ni-based cermets by plasma spraying on anode microstructural and chemical stability in dry methane

E. Lay, C. Metcalfe, O. Kesler*

Department of Mechanical and Industrial Engineering, University of Toronto, 5 King's College Road, Toronto, Ontario M5S 3G8, Canada

HIGHLIGHTS

► First fabrication of (Ni,Mg)O based cermets by solution precursor plasma spraying.
► Demonstration of reduced C deposition with MgO addition to cermet.
► Reduction in extent of Ni coarsening with MgO addition to cermet.

ARTICLE INFO

Article history:
Received 30 April 2012
Received in revised form
27 June 2012
Accepted 30 June 2012
Available online 7 July 2012

Keywords:
Anode
Cermet
Magnesia
Methane
Nickel
Solid oxide fuel cell

ABSTRACT

The Solution Precursor Plasma Spray (SPPS) process was successfully used to deposit cermet coatings that exhibit fine microstructures with high surface area. MgO addition in Ni-YSZ and Ni-SDC cermets results in (Ni,Mg)O solid solution formation, and nickel particles after reduction are finer than in coatings without magnesia. The influence of MgO on the chemical stability of cermets in anodic operating conditions is discussed. It was found that a sufficient amount of magnesia addition ($Ni_{0.9}(MgO)_{0.1}$) helps to reduce carbon deposition in dry methane.

1. Introduction

Solid oxide fuel cells (SOFCs) are promising devices for electricity generation. The most common anode material is a nickel-based cermet, for example, either Ni-YSZ (yttria-stabilized zirconia) or Ni-SDC (samaria-doped ceria) for SOFCs with YSZ or SDC electrolytes, respectively. These cermets display excellent catalytic properties for fuel oxidation and good electronic conductivity. However, they still suffer from a number of drawbacks, such as coarsening of nickel grains [1] and carbon deposition in hydrocarbon fuels [2]. In the latter case, active sites are covered with deposited carbon, resulting in the deactivation of the catalyst sites, and thus a loss of SOFC cell performance. Irreversible performance loss can occur when carbon dissolves in the Ni and then precipitates as carbon fibers, leading to disintegration by metal dusting. One way to prevent or suppress these modes of degradation is the incorporation of a third phase in the cermet. In particular, the addition of an alkaline earth oxide such as MgO may improve the stability of Ni-based cermets. Indeed, NiO–MgO solid solutions have been used for many years as catalysts for the carbon dioxide reforming of methane [3]. The use of MgO in supported nickel catalyst systems has been found to reduce carbon deposition during the steam reforming of methane [4].

In addition, NiO–MgO solid solutions exhibit good thermal stability due to their high metal dispersion, resulting in little coarsening of Ni particles after sintering [4–7], and the addition of 4 mol.% of MgO with respect to NiO results in suppression of Ni re-oxidation by inhibiting NiO–Ni particle shape changes during reduction–oxidation cycles [8]. Moreover, the high dispersion of Ni particles results in a high activity for reforming of methane [5,9].

In order to create a very fine microstructure of Ni and MgO in cermets in this work, a manufacturing process based on plasma spraying was employed. A wide range of manufacturing processes are used to produce planar and tubular SOFCs, such as screen

* Corresponding author. Tel.: +1 416 978 3835; fax: +1 416 978 7753.
E-mail address: kesler@mie.utoronto.ca (O. Kesler).

0378-7753/$ – see front matter © 2012 Elsevier B.V. All rights reserved.
http://dx.doi.org/10.1016/j.jpowsour.2012.06.106

printing, tape casting, vapor deposition, and plasma spraying [10,11]. Wet ceramic techniques require long processing times and high-temperature heat treatments. In contrast, plasma spraying is a rapid process that can be used to fabricate each of the active cell components, with many potential advantages such as rapid production, material compositional flexibility, and the elimination of the need for high-temperature sintering processes. These advantages can make the process particularly beneficial for the fabrication of metal-supported cells as a way to lower the material cost and increase the durability of the fuel cells.

In the case of traditional atmospheric plasma spraying (APS), dry powders are injected into a high temperature and high velocity plasma, accelerated, melted, and deposited on a substrate [12]. Plasmas used in the process typically have a high enthalpy density, high temperature, high velocity, and high heat transfer rates to the injected feedstock powders, making it possible to rapidly melt ceramic and metal feedstock powder particles in milliseconds. The process allows fully-consolidated coatings to be produced without sintering, which facilitates the use of otherwise incompatible materials, such as metal supports with electrolytes that would otherwise require high-temperature sintering or adjacent electrolyte and electrode materials that would otherwise inter-react during sintering but not during cell operation.

A wide range of spraying and process parameters can be controlled along with the powder properties to achieve desired coating properties. An alternative to the use of dry powders as feedstock is the use of liquid-based feedstock. Liquid feedstock can take the form of powders dispersed in a liquid (suspension plasma spraying, SPS [13,14]) or of homogeneously dissolved precursor materials in a solvent (solution precursor plasma spraying, SPPS [13–15]). These methods have the advantage of facilitating the use of finer feedstock particle sizes in the case of SPS or of atomically-mixed precursor feedstock in the case of SPPS, both of which have the potential to produce electrodes with finer structures without subsequent sintering. Moreover, SPPS is a simple, single-step and rapid technique for both synthesizing and depositing materials. The preparation of the feedstock is easier in SPPS than in methods using powder-based feedstock because there is no need for powder feedstock preparation such as agglomeration by spray drying or for dispersion of powders in suspensions.

This study aims to realize stable Ni-based SPPS-fabricated cermets. It thus deals with the fabrication method and the effect of MgO addition on both the coking resistance and the stability in operating conditions. Therefore, the present work aims to develop new and simpler manufacturing methods based on SPPS to fabricate anodes with improved performance compared to anodes with the same materials fabricated by wet ceramic techniques.

2. Experimental procedure

2.1. Feedstock preparation

The precursor solutions were obtained by dissolving stoichiometric amounts of $Ni(NO_3)_2 \cdot 6H_2O$ (98%), $Mg(NO_3)_2 \cdot 6H_2O$ (98%), $ZrOCl_2 \cdot 8H_2O$ (98%), $Y(NO_3)_3 \cdot 6H_2O$ (99.9%), $Ce(NO_3)_3 \cdot 6H_2O$ (99.5%) and $Sm(NO_3)_3 \cdot 6H_2O$ (99.9%) all from Alfa Aesar (Ward Hill, MA), in deionized water. Compositions of ceramic phases are 8 mol.% Y_2O_3 stabilized ZrO_2 for YSZ and $Sm_{0.15}Ce_{0.85}O_{2-y}$ for SDC, and the targeted metal to ceramic phase ratio is 40–60 vol.% after reduction. The targeted quantity of MgO is $(NiO)_{0.9}(MgO)_{0.1}$-YSZ and $(NiO)_{0.9}(MgO)_{0.1}$-SDC.

2.2. Spray parameters

Coatings were produced at atmospheric pressure using an Axial III Series 600 plasma torch (Northwest Mettech Corp., North Vancouver, BC, Canada). The plasma jet is generated by flowing gas across three separate cathode–anode pairs. The plasma gas is a mixture of nitrogen, argon and hydrogen, with their respective amounts influencing the plasma power and heat transfer properties. The liquid feedstock was injected axially, directly into the convergence of the three plasma jets. Nitrogen was used as an atomizing gas at a flow rate of 10 slpm. The torch was mounted on a robot and moved in a raster pattern in front of the substrates. The spray parameters used for the experiments are listed in Table 1.

Preliminary coatings were deposited onto 25.4 mm diameter porous stainless steel substrates (Mott Corporation, Framingham, CT, USA). SPPS coatings were reduced in a 40 vol.% H_2–60 vol.% N_2 mixture (total flow rate 250 sccm) at 600 °C for 3 h or at 700 °C for 5 h. Reduction was checked by X-ray diffraction (XRD) measurements.

2.3. Coating characterization

A Philips diffractometer (PW 1830 HT generator and PW 1050 goniometer) using Cu Kα radiation was used to determine the phases in the coatings. XRD patterns were recorded in the range $2\theta = 15–80°$, with 0.02° and 2.5 s angular and time steps, respectively. Scanning electron microscopy (SEM) coupled with energy-dispersive X-ray spectroscopy (EDS) was used to evaluate the morphology and elemental compositions of coatings, respectively, using (i) a JSM-840 JEOL microscope, complemented by a PGT/AAT EDS detector and an IXRF 500 digital pulse processor or (ii) a Hitachi S-4500 field emission microscope, complemented by an Oxford Instruments High Purity Germanium EDS Detector.

2.4. Coarsening experiment

A furnace test was realized at 850 °C for 72 h using a ramp rate of 10 °C min^{-1} in wet (3% H_2O) 5 vol.% H_2 in Ar (total flow rate 250 sccm) on Ni-SDC and $Ni_{0.9}(MgO)_{0.1}$-SDC prepared by spraying parameters SP1 in Table 1. The addition of MgO to Ni-YSZ cermets has been shown to prevent nickel particle coarsening by Chinarro et al. [7] and as such only MgO addition to Ni-SDC cermets has been investigated in this coarsening study.

2.5. Carbon deposition experiments

Coatings were heated in a tube furnace at 10 °C min^{-1} in 100% N_2 to 700 °C, at which point CH_4 was added at 40 vol.% for 2 h, followed by 100% CH_4 for an additional 1.5 h (total flow rate 250 sccm). The weight gain determined by subtracting the initial weight of the sample from the final weight closely represents the amount of carbon deposited on the sample.

Thermogravimetric analysis (TGA) experiments were realized using a SETSYS Evolution TGA device (Setaram). The sample was loaded into the TGA and purged at 200 sccm in N_2 for 10 min at room temperature, followed by 10 min at 31 sccm N_2. The

Table 1
Summary of spraying parameters.

	SP1	SP2
Ni^{2+} concentration (±0.02 mol L^{-1})	0.70	1.50
Nozzle size (mm)	14.3	14.3
Standoff distance (±2 mm)	150	90
Plasma gas flow rate (±5 slpm)	250	175
Plasma gas composition (vol.%)	15% Ar	30% Ar
	80% N_2	65% N_2
	5% H_2	5% H_2
Torch arc current (±2 A cathode^{-1})	200	200
Feedstock feed rate (±2 g min^{-1})	100	50
Total plasma torch power (±2 kW)	126	100

temperature was then increased under the latter gas atmosphere to 700 °C at 50 °C min^{-1}. The sample was then exposed to 4.8 vol.% CH_4 balance N_2 at a total flow rate of 31 sccm for 15 h. The temperature was subsequently reduced to lab temperature at 25 °C min^{-1} under the same gas atmosphere (4.8 vol.% CH_4).

The mass flow controllers (Alicat Scientific Inc., Tucson, AZ.) used for the coarsening experiment and carbon deposition experiments have a full scale of 250 sccm and were factory calibrated with accuracy specified to ±0.8% of reading or 0.2% of full scale, whichever is greater.

3. Results and discussion

3.1. Phase formation

Addition of nickel cations in the precursor solution along with the cations in the fluorite phases leads to the formation of NiO and the desired fluorite ceramic phase, as seen in Fig. 1(a) for NiO-YSZ and in Fig. 2(a) for NiO-SDC. Figs. 1(b) and 2(b) are XRD patterns of $(NiO)_{0.9}(MgO)_{0.1}$-YSZ and $(NiO)_{0.9}(MgO)_{0.1}$-SDC coatings after deposition, respectively. MgO and NiO peaks are not readily distinguishable. However, even though the MgO and NiO XRD patterns are similar, doublet peaks corresponding to both phases appear on XRD patterns of a mixture of NiO and MgO powders without any calcination [16]. Although the lattice parameters in plasma-sprayed coatings typically deviate from the stress-free lattice parameters due to residual stresses, the absence of doublets suggests the formation of a solid solution of NiO and MgO, (Ni,Mg)O. Indeed, MgO and NiO have similar lattice parameters (4.213 Å and 4.1769 Å in their stress-free states, respectively [17]) and bond distances, and can form a solid solution [6]. A reduction step at 700 °C for 5 h using a ramp rate of 10 °C min^{-1} in a H_2–N_2 mixture leads to the targeted phases of Ni metal, MgO, and YSZ or SDC (Figs. 1(c) and 2(c)). Except for the coatings whose XRD patterns are shown in Fig. 2(a) and (c), which were fabricated with conditions SP1, the XRD patterns are from coatings fabricated using spraying conditions that differ slightly from the SP1 conditions.

3.2. Microstructure of the coatings

Coatings realized by SPPS exhibit fine microstructures with high surface area (Figs. 3 and 4). This feature may lead to a large electrocatalytic reaction zone and allows a good gas supply network, which are the main requirements for a high-performance electrode [18].

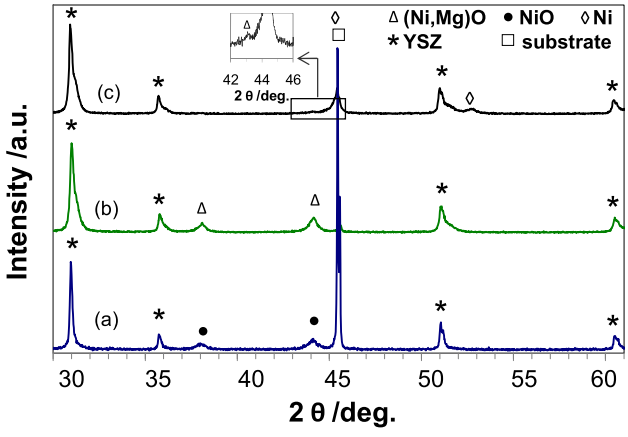

Fig. 1. XRD patterns of coatings composed of (a) NiO-8YSZ using spraying conditions SP1 modified to have a 180 mm standoff distance, (b) $(NiO)_{0.9}(MgO)_{0.1}$-YSZ using spraying conditions SP2 and (c) $Ni_{0.9}(MgO)_{0.1}$-YSZ using spraying conditions SP2 and deposited on stainless steel substrates.

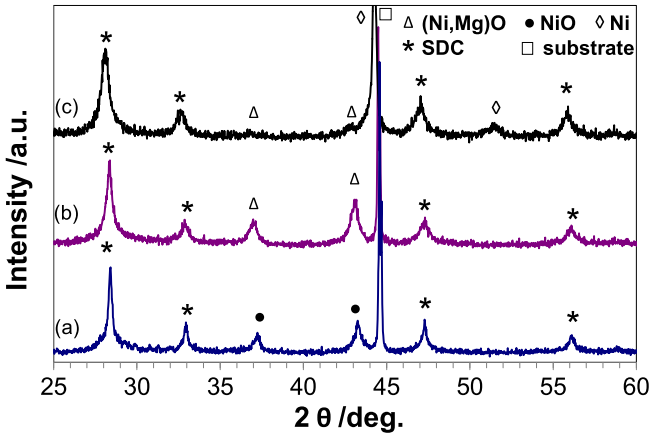

Fig. 2. XRD patterns of coatings composed of (a) NiO-SDC using spraying conditions SP1, (b) $(NiO)_{0.9}(MgO)_{0.1}$-SDC using spraying conditions SP1 and (c) $Ni_{0.9}(MgO)_{0.1}$-SDC using spraying conditions SP1 modified to have 0% H_2, 250 A cathode^{-1} and a 100 mm standoff distance. All coatings sprayed on stainless steel substrates.

Two sets of parameters were used to spray Ni-SDC based coatings. The plasma generated with the first set of spray parameters (SP1) has a higher velocity and higher energy than that produced with the second set of parameters (SP2). However, the precursor solution flow rate is also higher, while the concentration is smaller. A Ni-SDC coating (Fig. 4(b)) presents a similar microstructure as Ni-YSZ (Fig. 3(a)), but with a larger quantity of finer particles.

Coating morphology depends on the set of parameters used for spraying. In the high-temperature plasma jet, the solution droplets undergo a series of physical changes and chemical reactions prior to deposition on the substrate, including evaporation of the water and formation of the oxide phases. Depending on the plasma spraying conditions, different phenomena may occur during these steps [19–22].

The precursor solution is atomized into multiple precursor droplets, with a wide size distribution of the droplets. The solvent in the droplets, which in our case is water, undergoes rapid evaporation, increasing the concentration of solute. These processes are followed by precipitation, gelation, and pyrolysis. Pyrolysis can occur either in the plasma or *in situ* on the substrate if the unpyrolysed droplet had previously impacted the substrate. The unpyrolysed gel-like precursors incorporated into the coating pyrolyze and form aggregates of solid particles when subsequently heated by additional passes of the plasma torch. Pyrolysis and crystallization can also occur before the substrate impact, with droplets undergoing crystallization and then melting in the plasma. Splats are formed when the molten droplets impact on the substrate, and spherical particles could be formed if the droplet is just partially melted (on the surface) or has resolidified and is incorporated into the coating by surrounding melted material.

The absence of splat-shaped microstructural features or even spherical particles for Ni-SDC sprayed with the set of parameters SP1 is evidence that little melting of droplets occurred in the plasma. This observation is consistent with the fact that the solution concentration is lower for spray conditions SP1 than for spray conditions SP2 ($[Ni^{2+}]_{SP1} = 0.7$ mol L^{-1} for the set of parameters SP1 compared to $[Ni^{2+}]_{SP2} = 1.5$ mol L^{-1} for the set of parameters SP2).Thus, it is highly possible that most of the elements were vaporized in the plasma, and then subsequently nucleated at the surface of the substrate. This kind of coating is inherently less adherent to the substrate, which is detrimental for the long term stability. Despite the poorer adherence, stability tests were performed on materials fabricated with the set of spray parameters

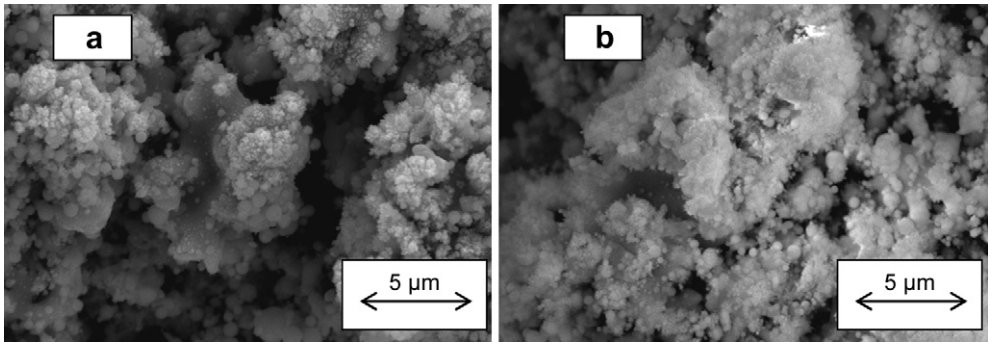

Fig. 3. Scanning-electron micrographs of (a) Ni-YSZ and (b) $Ni_{0.9}(MgO)_{0.1}$-YSZ prepared by SPPS using spraying parameters SP2, after reduction.

SP1 to determine the impact of the MgO addition on microstructural coarsening.

Magnesium oxide incorporation results in a larger quantity of finer particles both for Ni-YSZ (Fig. 3(b)) and Ni-SDC (Fig. 4(c) and (d)) based coatings, which is consistent with results observed in previous studies in which the materials were synthesized by wet ceramic processes [4–6,23].

3.3. Stability test

A higher dispersion of Ni particles could lead to a possible improvement of the thermal stability [4]. Indeed, one of the Ni-based cermet degradation mechanisms is the coarsening of nickel grains at operating temperatures, which leads to a disruption of the percolation path. The coatings fabricated by SPPS initially present a high dispersion of nickel particles. To investigate the stability of the microstructure at operating temperatures, the influence of the microstructure and of MgO content on the stability was investigated. Fig. 5 presents SEM micrographs of two coatings heated at 850 °C for 72 h in wet (3 vol.% H_2O) 5 vol.% H_2 in Ar, one with and one without MgO. Both of the samples contain some larger particles of nickel after heating at 850 °C, showing that nickel coarsened somewhat during the heating step. However, the final microstructural feature sizes and the extent of coarsening qualitatively appear to be smaller when MgO is present (Fig. 5(c) and (d)), compared to when MgO is absent (Fig. 5(a) and (b)). As a consequence, MgO might have a positive influence in helping to prevent nickel coarsening.

3.4. Carbon deposition

A stability test in methane was realized in dry conditions (40 vol.% CH_4 in N_2, followed by pure methane). In these conditions, the primary reaction potentially leading to coking is methane cracking:

$$CH_4 \rightarrow C + 2H_2 \quad (1)$$

Fig. 6 presents coating micrographs after exposure to dry methane. As seen in Fig. 6(a) and (b), both Ni-YSZ based coatings present some fine carbon fibers, with the $Ni_{0.9}(MgO)_{0.1}$-YSZ

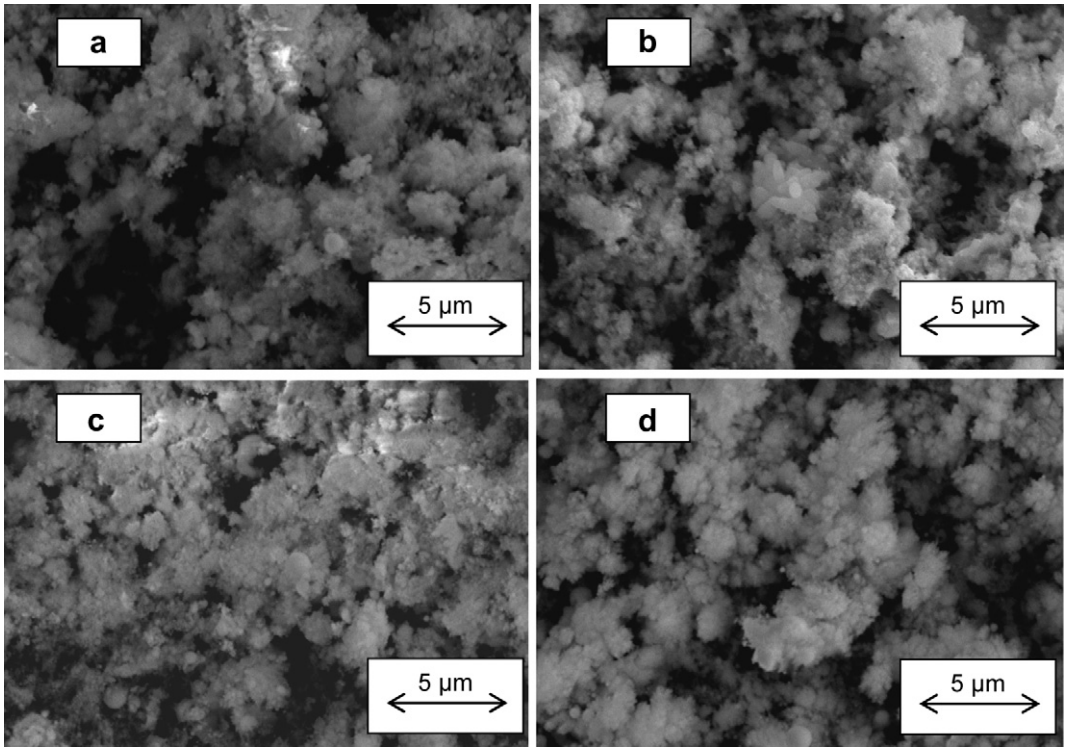

Fig. 4. Scanning-electron micrograph of (a) Ni-SDC (SP1), (b) Ni-SDC (SP2), (c) $Ni_{0.9}(MgO)_{0.1}$-SDC (SP1), (d) $Ni_{0.9}(MgO)_{0.1}$-SDC (SP2) prepared by SPPS with spraying parameters SP1 or SP2, after reduction.

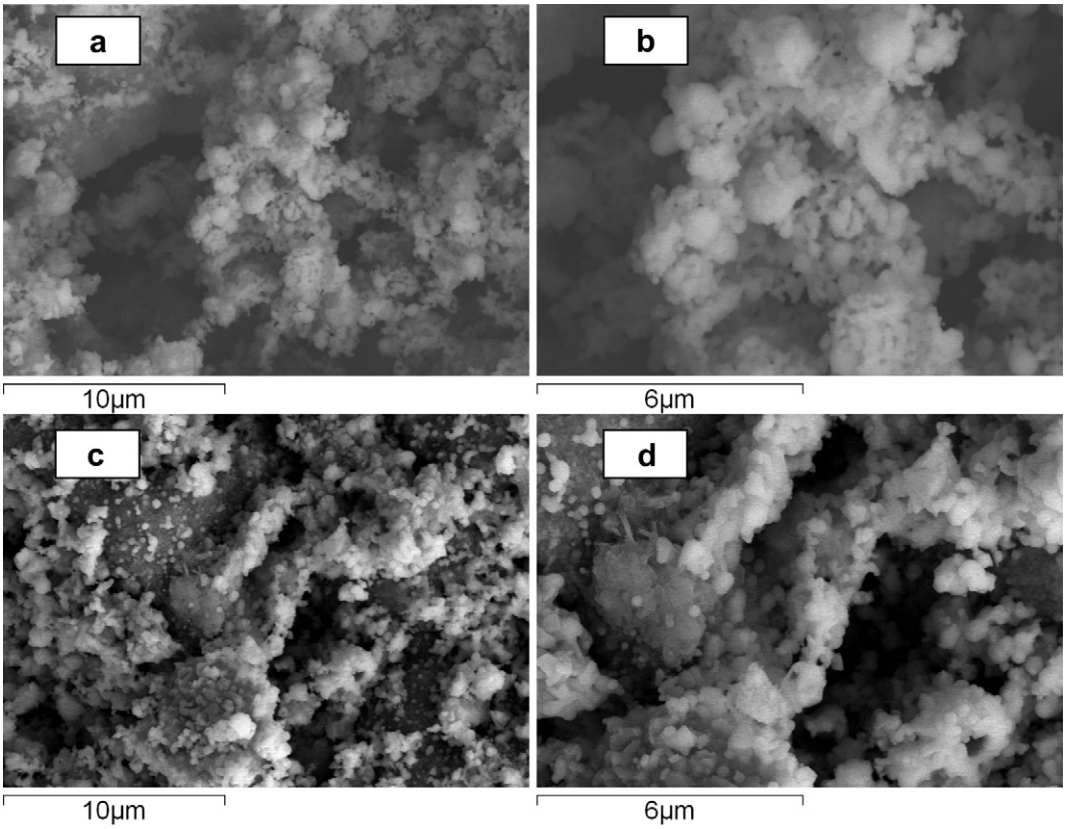

Fig. 5. Scanning-electron micrograph of (a) and (b) Ni-SDC, (c) and (d) $Ni_{0.9}(MgO)_{0.1}$-SDC prepared by SPPS with spraying parameters SP1 after heating at 850 °C for 72 h in wet (3% H_2O) 5 vol.% H_2 in Ar. (a) and (c): lower magnification; (b) and (d): higher magnification.

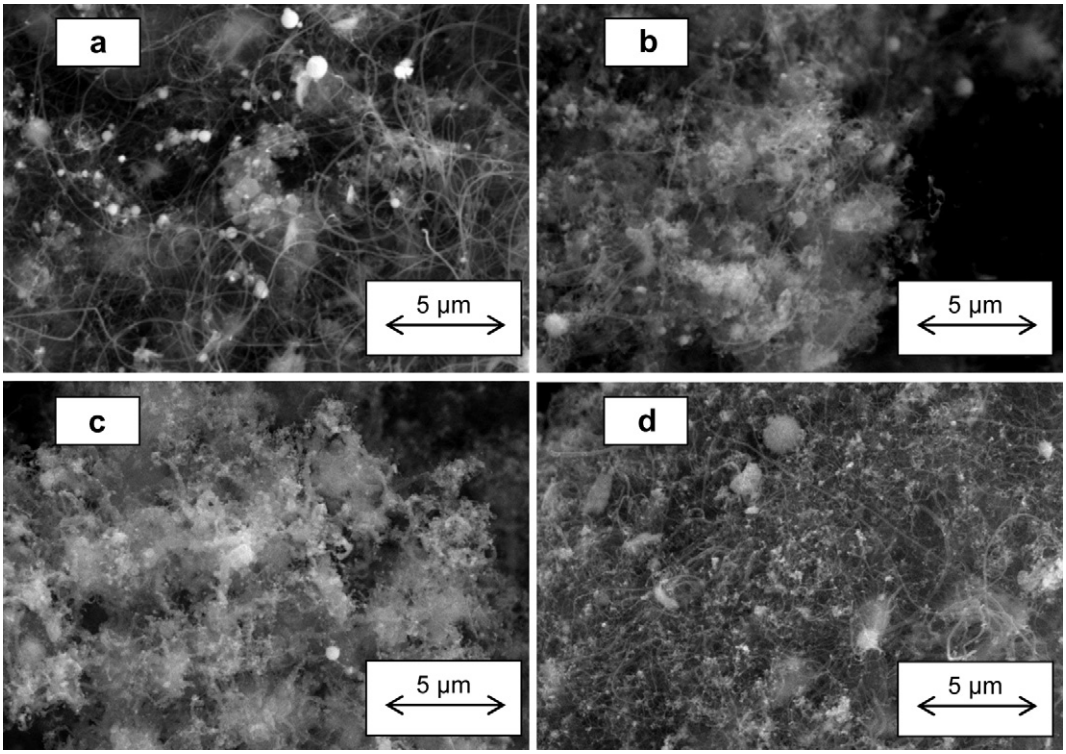

Fig. 6. Scanning-electron micrograph of (a) Ni-YSZ, (b) $Ni_{0.9}(MgO)_{0.1}$-YSZ, (c) Ni-SDC and (d) $Ni_{0.9}(MgO)_{0.1}$-SDC after CH_4 exposure test at 700 °C (40 vol.% CH_4 in N_2, followed by pure methane).

showing substantially fewer carbon fibers, whereas Ni-SDC (Fig. 6(c)) and $Ni_{0.9}(MgO)_{0.1}$-SDC (Fig. 6(d)) show different methane responses from those of the Ni-YSZ and $Ni_{0.9}(MgO)_{0.1}$-YSZ coatings. While both the Ni-SDC and $Ni_{0.9}(MgO)_{0.1}$-SDC have visible carbon fibers, the carbon fibers are coarser on the Ni-SDC coating than on the $Ni_{0.9}(MgO)_{0.1}$-SDC coating. The diameters of the observed carbon fibers are generally similar to the size of the Ni particles [24], which is consistent with the dispersion effect of MgO on Ni particles. Table 2 reports the quantity of carbon deposited during the stability tests in methane compared to both the total coating weight after reduction and the Ni content. Addition of magnesium oxide by spraying with parameters SP2 improves the coking resistance for both Ni-SDC and Ni-YSZ.

A similar amount of carbon deposition has been reported on $(NiO)_{0.9}(MgO)_{0.1}$-SDC after a test in dry methane at 750 °C [25]. Since the size of Ni particles in SPPS coatings is already in the submicrometer range, it may be that the addition of MgO slowed the sintering process of the nickel particles, and may have interfered with the formation and deposition of long carbon fibers by separating the catalytic reaction sites on Ni [26], potentially thereby slowing down the rate at which the carbon fibers could form on the nickel catalyst.

A carbon deposition test was also performed on a sample that contains less magnesia, $Ni_{0.97}(MgO)_{0.03}$-YSZ, with carbon weight gain monitored by TGA (Fig. 7). As one can see in Fig. 7, the addition of the smaller amount of MgO results in an increase in coking, with a higher rate of carbon deposition for the first 2 h. After several hours, both specimens slowed in their rate of carbon deposition. In the dry methane conditions tested, reaction (1) is probably the reaction occurring. When the rate of coking drops and the carbon weight approaches a plateau, an equilibrium is achieved between the formation of coke (1) and its gasification.

This experimental result is in agreement with a furnace test realized in wet (3% H_2O) 4 vol.% CH_4 in N_2 (S/C = 0.75) at 700 °C on similar materials. After 3 h in these conditions, the weight gain due to carbon was +107 wt.% for the Ni-YSZ coating and +345 wt.% for the $Ni_{0.97}(MgO)_{0.03}$-YSZ, with respect to Ni weight. After 3 h in dry methane during the TGA experiment (Fig. 7), the weight gain due to carbon was +161 wt.% for the Ni-YSZ coating and +426 wt.% for the $Ni_{0.97}(MgO)_{0.03}$-YSZ, with respect to Ni weight. The weight gain decreases with the addition of steam, because steam reforming (2) is likely occurring, along with water–gas shift (3), thus reducing the amount of CH_4 that pyrolyzes to deposit carbon:

$$CH_4 + H_2O = CO + 3H_2 \quad (2)$$

$$CO + H_2O = CO_2 + H_2 \quad (3)$$

In the experiments both with and without 3% H_2O added, carbon deposition increased by at least a factor of two when a small quantity of MgO (3 mol.% compared to Ni) was present in the coating. This result shows that a minimum amount of MgO is necessary to prevent carbon deposition. A previous study [27] shows that the carbon deposition extent depends on the MgO quantity, but does not follow a proportional trend. The authors studied the stability of $Ni_{1-x}(MgO)_x$ with $x = 0.13, 0.42, 0.59$. In that study, there was a decrease in carbon deposition with increasing content of MgO, but the optimum values were $x = 0.13$ and 0.59 wt.%, and the carbon weight gain was higher for $x = 0.42$ (but smaller than for $x = 0$).

Table 2
Carbon quantity deposited on the coatings with respect to nickel weight in the coatings after exposure to dry methane at 700 °C.

Sample	Ni-YSZ based cermet (wt.% C w.r.t Ni)	Ni-SDC based cermet (wt.% C w.r.t. Ni)
Without MgO	641 ± 46	283 ± 20
With MgO	340 ± 27	58 ± 10

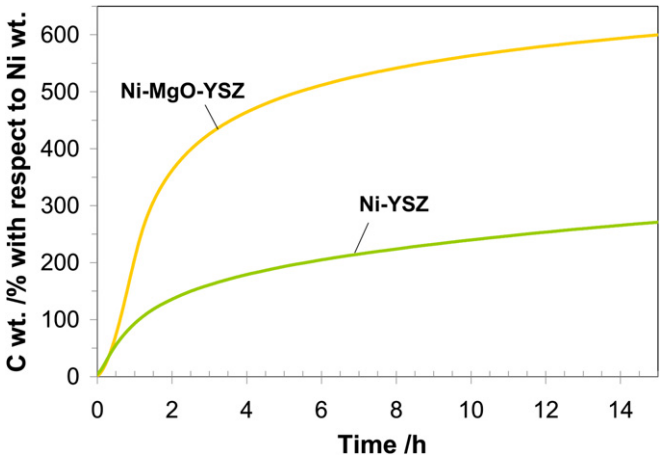

Fig. 7. TGA experiment in 4% CH_4 in N_2 at 700 °C realized on $Ni_{0.97}(MgO)_{0.03}$-YSZ and Ni-YSZ.

An optimization study of the amount of magnesia in the coating must be performed to identify the best amount for anodes made by each fabrication process.

The basicity properties of MgO have been found to improve the CH_4 reforming activity by promoting interaction with reactant gases such as H_2O and/or CO_2 [6,28]. Also, the basic catalyst promotes the steam gasification reaction between steam and carbon (4):

$$C + H_2O = CO + H_2 \quad (4)$$

This phenomenon occurs for both small and large MgO amounts. For example, carbon deposition was reported in CH_4–N_2 on $Ni_{0.03}Mg_{0.97}O$ at 500 °C for 2 h [6], while little deposited coke (<1.0 wt.%) was formed on the solid solution $Ni_{0.032}Mg_{0.968}O$ catalyst over 65 h of steam reforming of methane (S/C = 1) [29]. Asamoto et al. [30] reported that introducing MgO in a Ni/SDC ($Ni_{0.87}(MgO)_{0.13}$ composition) anode has no effect on reducing the extent of carbon deposition compared to Ni-SDC in dry methane. However, no carbon formation was obtained on a reduced $Ni_{0.1}(MgO)_{0.9}$ catalyst after a test in 50 vol.% CO_2–50 vol.% CH_4 for 120 h [31].

The decrease in coke formation and deposition even in dry methane observed in this study for specimens made with 10 mol.% MgO compared to Ni could be linked to 2 mechanisms:

(i) The added basic metal oxide might cover a part of the Ni metal surface; the oxide might thereby block Ni sites for nucleation of carbon. Indeed, the cracking reaction requires a large ensemble of Ni surface sites [26].
(ii) The added basic metal oxides increase the electron density of the Ni metal [27,32]. This electronic enrichment results in a higher affinity of metal particles toward electron-attractor C and O species, thereby depressing the reactivity of the Ni/MgO system in the Boudouard reactions. As a consequence, the kinetics of coke formation might be slower than that of carbon gasification, preventing extensive coking of the catalyst surface [32].

4. Conclusions

Solution precursor plasma spraying is a coating technique that combines the synthesis and the consolidation processes into a single step. The process saves time and avoids some of the problems, such as inter-reaction, encountered during conventional

wet ceramic deposition procedures. This method was used in this study to fabricate Ni-based cermet coatings with the addition of MgO. MgO addition in Ni-YSZ and Ni-SDC cermets results in solid solution (Ni,Mg)O formation, and nickel particles are finer than without magnesia. The influence of MgO on the chemical stability of cermets in anodic operating conditions is also discussed, with MgO reducing the amount of carbon deposited relative to the nickel content for the anodes deposited using spray conditions SP2, when the MgO is present in quantities of 10 mol.% relative to the Ni.

Acknowledgments

The authors gratefully acknowledge financial support from the Natural Sciences and Engineering Research Council (NSERC) of Canada and Northwest Mettech Corporation, as well as from the Solid Oxide Fuel Cell Canada Strategic Research Network sponsored by NSERC and other sponsors listed at www.sofccanada.com.

References

[1] D. Simwonis, F. Tietz, D. Stöver, Solid State Ionics 132 (2000) 241–251.
[2] S.P. Jiang, S.H. Chan, J. Mater. Sci. 39 (2004) 4405–4439.
[3] Y.-H. Wang, H.-M. Liu, B.-Q. Xu, J. Mol. Catal. A: Chem. 299 (2009) 44–52.
[4] S. Wang, G.Q.M. Lu, Appl. Catal. B 16 (1998) 269–277.
[5] Y. Shiratori, Y. Teroka, K. Sasaki, Solid State Ionics 177 (2006) 1371–1380.
[6] K. Tomishige, Y. Chen, K. Fujimoto, J. Catal. 181 (1999) 91–103.
[7] E. Chinarro, F.M. Figueiredo, G.C. Mather, J.R. Jurado, J.R. Frade, J. Eur. Ceram. Soc. 27 (2007) 4233–4236.
[8] N.M. Tikekar, T.J. Armstrong, A.V. Virkar, J. Electrochem. Soc. 153 (2006) A654–A663.
[9] D.J. Moon, J.W. Ryu, Catal. Today 87 (2003) 255–264.
[10] S.C. Singhal, K. Kendall, High Temperature Solid Oxide Fuel Cells: Fundamental, Design and Applications, Elsevier, Oxford, UK, 2003.
[11] R. Hui, Z. Wang, O. Kesler, L. Rose, J. Jankovic, S. Yick, R. Maric, D. Ghosh, J. Power Sources 170 (2007) 308–323.
[12] O. Kesler, P. Marcazzan, in: J.W. Fergus, J. Zhang, X. Li, D.P. Wilkinson, R. Hui (Eds.), Solid Oxide Fuel Cells: Materials Properties and Performance, CRC Press, New York, 2009, pp. 239–282.
[13] P. Fauchais, R. Etchart-Salas, C. Delbos, M. Tognonvi, V. Rat, J.F. Coudert, T. Chartier, J. Phys. D: Appl. Phys. 40 (2007) 2394–2406.
[14] L. Pawlowski, Surf. Coat. Technol. 203 (2009) 2807–2829.
[15] G.-J. Yang, C.-J. Li, Y.-Y. Wang, J. Therm. Spray Technol. 14 (2005) 480–486.
[16] S. Tang, J. Lin, K.L. Tan, Catal. Lett. 51 (1998) 169–175.
[17] A. Kuzmin, N. Mironova, J. Phys.: Condens. Matter. 10 (1998) 7937–7944.
[18] H. Uchida, S. Suzuki, M. Watanabe, in: S.C. Singhal, M. Dokyia (Eds.), SOFC VIII, vol. 2003–2007, Electrochemical Society, Pennington, NJ, 2003, pp. 728–736.
[19] D. Chen, E.H. Jordan, M. Gell, Surf. Coat. Technol. 202 (2008) 2132–2138.
[20] D. Chen, E.H. Jordan, M. Gell, J. Mater. Sci. 42 (2007) 5576–5580.
[21] L. Xie, X. Ma, E.H. Jordan, N.P. Padture, D.T. Xiao, M. Gell, Surf. Coat. Technol. 177–178 (2004) 103–107.
[22] T. Bhatia, A. Ozturk, L. Xie, E.H. Jordan, B.M. Cetegen, M. Gell, X. Ma, N.P. Padture, J. Mater. Res. 17 (2002) 2363–2372.
[23] W. Gac, A. Denis, T. Borowiecki, L. Kepinski, Appl. Catal. A 357 (2009) 236–243.
[24] T. Takeguchi, Y. Kani, T. Yano, R. Kikuchi, K. Eguchi, K. Tsujimoto, Y. Uchida, A. Ueno, K. Omoshiki, M. Aizawa, J. Power Sources 112 (2002) 588–595.
[25] M. Phongaksorn, Ph.D. Thesis, University of Waterloo, Canada, 2010.
[26] D.L. Trimm, Catal. Today 49 (1999) 3–10.
[27] T. Horiuchi, K. Sakuma, T. Fukui, Y. Kubo, T. Osaki, T. Mori, Appl. Catal. A 144 (1996) 111–120.
[28] J. Requies, M.A. Cabrero, V.L. Barrio, M.B. Güemez, J.F. Cambra, P.L. Arias, F.J. Pérez-Alonso, M. Ojeda, M.A. Peña, J.L.G. Fierro, Appl. Catal. A 289 (2005) 214–223.
[29] O. Yamazaki, K. Tomishige, K. Fujimoto, Appl. Catal. A 136 (1996) 49–56.
[30] M. Asamoto, S. Miyake, K. Sugihara, H. Yahiro, Electrochem. Commun. 11 (2009) 1508–1511.
[31] E. Ruckenstein, Y.H. Hu, Appl. Catal. A 133 (1995) 149–161.
[32] F. Frusteri, F. Arena, G. Calogero, T. Torre, A. Parmaliana, Catal. Commun. 2 (2001) 49–56.